Construction and Building Materials 48 (2013) 485–498

Contents lists available at ScienceDirect

Construction and Building Materials

journal homepage: www.elsevier.com/locate/conbuildmat

Review

Flexural strengthening of reinforcement concrete beams using high performance fiber reinforcement cement-based composite (HPFRCC) and carbon fiber reinforced polymers (CFRP)

Vladimir José Ferrari [a,*], João Bento de Hanai [b], Rafael Alves de Souza [a]

[a] Universidade Estadual de Maringá, UEM, Departamento de Engenharia Civil, Av. Colombo, 5.790, CEP 87.020-900 Maringá, PR, Brazil
[b] Universidade de São Paulo, Escola de Engenharia de São Carlos, EESC/USP, Av. Trabalhador São-Carlense 400, CEP 13.566-590 São Carlos, SP, Brazil

HIGHLIGHTS

- An innovative procedure for the flexure strengthening of RC beams is proposed.
- A high performance fiber reinforced cement-based composite (HPFRCC) was developed.
- The developed composite is able to constitute a better transition layer for CFRP sheets.
- The premature debonding of the CFRP sheets is avoided with this new procedure.
- The cracking pattern is also enhanced with the proposed methodology.

ARTICLE INFO

Article history:
Received 20 February 2013
Received in revised form 10 July 2013
Accepted 15 July 2013

Keywords:
Reinforced concrete
Strengthening
Carbon fibers
Steel fibers concrete
Fracture mechanics

ABSTRACT

This paper presents a strengthening method using a combination of high performance fiber reinforced cement-based composite (HPFRCC) and carbon fiber reinforced polymers (CFRP). For evaluating the performance of this approach, reinforced concrete (RC) beams strengthened with CFRP sheets have been tested to failure. In order to better control the cracking of concrete and prevent/delay the debonding of the CFRP sheets, a high performance material based on HPFRCC with specially designed microfibers has been mixed to be applied in a transition layer. As a result, a material with pseudo strain-hardening behavior, high strength and fracture toughness has been obtained. The application of the CFRP in the transition layer surface constituted by HPFRCC significantly improved the performance of the tested specimens. Results show that this technique may provide a safer alternative for the flexure strengthening of RC beams.

Contents

* Corresponding author. Tel.: +55 44 3011 1336.
E-mail address: vladimirjf@hotmail.com (V.J. Ferrari).

0950-0618/$ - see front matter © 2013 Elsevier Ltd. All rights reserved.
http://dx.doi.org/10.1016/j.conbuildmat.2013.07.026

1. Introduction

Durability, maintenance, retrofitting and strengthening of structures are some issues that have been gaining great prominence on the international scene. Nowadays it is not rare to find buildings with life cycles below their expectations which are even operating within the limits of stability and security (some bridges or viaducts, for example). The lack of simple procedures such as periodic inspections and preventive maintenance only makes this situation worse, which in turn culminates in a need for retrofitting, strengthening and sometimes the total demolition of the affected structures.

Strengthening of reinforced concrete (RC) structures based on the application of carbon fiber reinforced polymer (CFRP) has become an accepted solution in the last decades, presenting many advantages, such as high strength-to-weight ratio, corrosion resistance, and relative ease of application.

Despite the mentioned advantages, there are still some issues regarding the performance of the transition layer between the CFRP sheets and the concrete substrate. It is well known [1–3] that RC beams strengthened with CFRP sheets are susceptible to extremely undesirable brittle failure, which makes the total utilization of the tensile properties of the polymer impossible.

Such form of failure anticipates the collapse of strengthened beams due to the lack of strength mechanisms for transferring forces. One of these mechanisms is due to the localized debonding of the strengthening ("peeling off"), especially in the anchoring zone or zones with excessive concentration of flexural and/or shear cracks. More significant increments of resistance only can be achieved if the premature forms of failure are prevented [4].

In this way, the present paper aims at presenting a technique for the flexural strengthening of RC beams, based on the application of a high performance cement-based composite of steel fibers (HPFRCC) and microfibers for constructing a more effective transition layer. As shown in Fig. 1, the proposed transition layer may rebuild the tension zone of the reinforced concrete beams in order to better explore the properties of the strengthening using CFRP sheets. It should be highlighted that the microfibers used herein are not available in the market and they were specially developed for this research. Therefore, the results that will be shown ahead were not published before; these results are unique and may inspire new investigations worldwide.

As illustrated in Fig. 2, the proposed intervention is based on the withdraw of a certain region of the tensile zone of beams (bottom

Fig. 2. RC beams with tensile zone damaged by effect of corrosion ([5]).

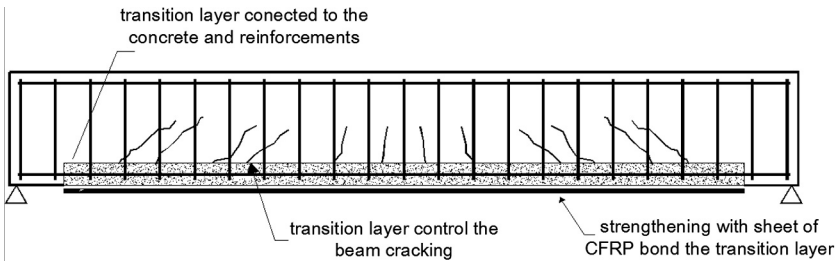

Fig. 1. Scheme of strengthening with CFRP sheets adhered to HPFRCC transition layer.

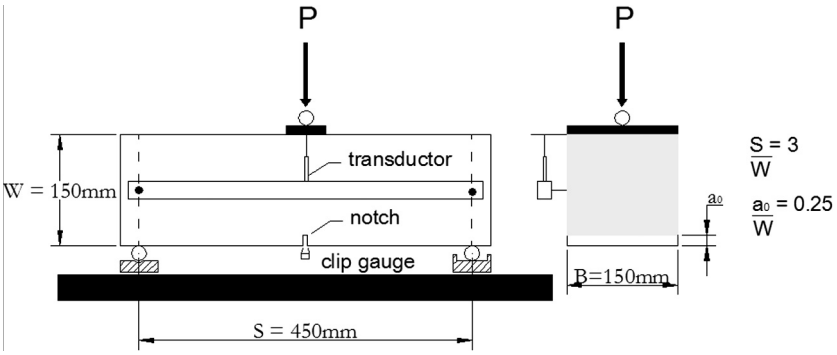

Fig. 3. General setup of the three bending point test of prismatic specimens.

chord) to be strengthened (frequently due to mechanical actions, corrosion or natural wear) and its subsequent reconstruction using HPFRCC. Thus, it is supposed that the reconstructed bottom chord of the beam could constitute a transition substrate with more appropriate characteristics for the flexure strengthening using CFRP sheets.

2. High performance cement-based composite

According to Ref. [5], the modifications resulting from the addition of steel fibers to concrete, at relatively low rates (a maximum of 2%), are restricted only to the post-peak stage of the loading history. According to Ref. [6], under such conditions, the steel fibers are not sufficient to inhibit the matrix cracking process which precedes the maximum load (subcritical growth of cracks).

In order to improve the cement-based composite behavior during the pre-peak stage, steel microfibers were incorporated to the matrix rather than using conventional steel fibers. In this way, a modification of the microstructure of the composite has been made, improving the process of stress transfer from the matrix to the fibers.

In this section, the experimental methodology and the obtained results in the development of a cement-based composite for reconstructing the tensile zones of RC beams are presented. At first glance, the developed composite is able to constitute a better transition layer, improving the cracking control and postponing the premature debonding of the polymeric strengthening.

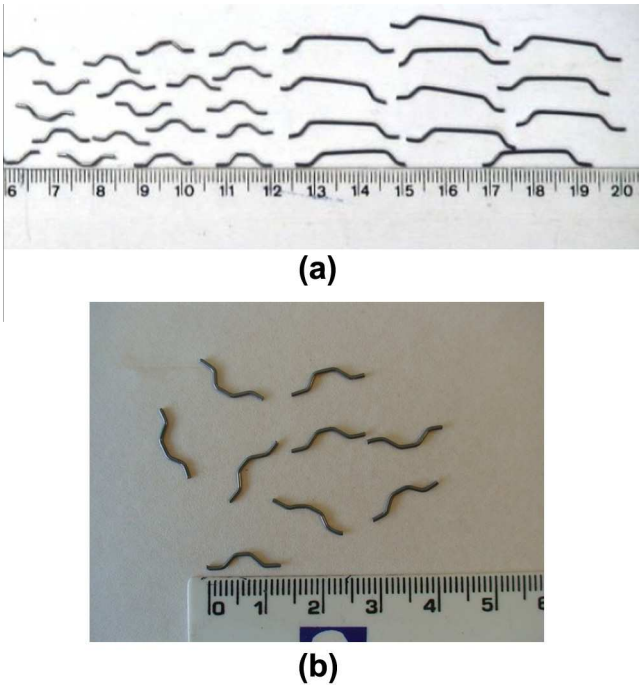

Fig. 4. Steel fibers. (a) Fibers A and C. (b) Fiber C: detail.

2.1. Test setup

In order to evaluate the tensile strength of the developed cement-based composite, the three point bending test of prismatic specimens with central notch as recommended by Ref. [7] has been applied. In Fig. 3 it is possible to visualize the general aspect of the test setup. The tests were conducted by controlling the crack mouth opening displacement (CMOD), by means of a clip gauge.

Table 1
Composites analyzed.

	Group	Composites	Fiber volume	Fiber type	Age	[a] E_c (GPa)
Mortar (A)	1	CPA	0%	–	29 days	24
	2	CPA1A	1%	A	29 days	23
	3	CPA1.5A	1.5%	A	29 days	23
	4	CPA2A	2%	A	29 days	24
	5	CPA1.5A0.5C	1.5% + 0.5%	A + C	28 days	28
	6	CPA1.5A1.5C	1.5% + 1.5%	A + C	28 days	32
	7	CPA1.5A2.5C	1,5% + 2.5%	A + C	28 days	31
	8	CPA1.5A3.5C	1.5% + 3.5%	A + C	28 days	29
Microconcrete (M)	9	CPM	0%	–	28 days	35
	10	CPM1A	1%	A	28 days	31
	11	CPM1A1C	1% + 1%	A + C	28 days	26
	12	CPM1A2C	1% + 2%	A + C	28 days	30
	13	CPM1A2.5C	1% + 2.5%	A + C	28 days	20

[a] E_c: elastic modulus.

2.2. Composites analyzed

Thirteen composites, each with different characteristics obtained from the variation of the rate and type of steel fibers used, have been analyzed. This set was divided into groups formed by three prisms (150 mm × 150 mm × 500 mm) molded with the same characteristics, as presented in Table 1.

The specimens have been divided into two steps according to the type of cement matrix, mortar, and microconcrete used. In order to produce the cementitious matrix of mortar and microconcrete the following materials have been used: Portland cement of high early strength and density of 3.15 g/cm^3, medium sand with a fineness modulus of 2.68 and an apparent specific gravity of 2.65 g/cm^3, and a maximum aggregate size of 10 mm and a particle density of 2.87 g/cm^3. A superplasticizer that acts as a dispersant of the cementitious material has also been used and all composites had 0.5% of superplasticizer by weight of cement. The cement consumption for the mortar and microconcrete was 512 kg/m^3 and 446 kg/m^3, respectively. The steel fiber specified as "A" has been provided by the company Maccaferri–Latin America and has a length of 25 mm, hooks at the ends and a diameter of 0.75 mm (trade name FS8-Wirand). On the other hand, the steel fiber "C", provided by the same manufacturer, has a length of only 13 mm, hooks at the ends and a diameter of 0.75 mm. The two types of fibers used in this research are showed in Fig. 4. Its interesting to point out that steel fiber "C" was specially developed for this experimental research.

2.3. Results of flexural tests on three points

2.3.1. Loads and strengths

In order to determine the flexural toughness of the composites, the recommendations prescribed by the work group TC 162-TDF of RILEM [7] have been followed. In Table 2, values of loads and resistance calculated based on these recommendations are presented.

For mortar composites, the addition of fibers has increased the limit of proportionality ($f_{fct,L}$). For these composites the matrix contribution in terms of strength was increased with the incorporation of steel fibers. The hybrid composites with the addition of steel microfibers of type C and fibers type A, werethose with higher values $f_{fct,L}$ among all the composite cement-based mortar analyzed.

Table 2
Load and strength according to RILEM [7].

Composite	Loads (kN)				Strengths (MPa)				
	F_L	F_M	$F_{R,1}$	$F_{R,4}$	$f_{fct,L}$	$f_{eq,2}$	$f_{eq,3}$	$f_{R,1}$	$f_{R,4}$
CPA	8.0	8.0	1.3	–	2.3	–	–	0.4	–
CPA1A	13.4	13.4	12.5	5.2	3.9	3.3	2.6	3.6	1.5
CPA1.5A	13.2	16.1	16.0	6.1	3.7	4.6	3.2	4.5	1.7
CPA2A	14.5	17.8	17.4	7.6	4.6	5.5	4.2	5.5	2.4
CPA1.5A0.5C	16.4	17.8	17.2	9.3	4.6	4.9	4.0	4.8	2.6
CPA1.5A1.5C	16.0	21.0	20.9	9.4	4.8	6.5	4.8	6.3	2.8
CPA1.5A2.5C	22.1	23.7	23.5	12.8	6.1	6.5	5.0	6.5	3.6
CPA1.5A3.5C	20.0	21.4	20.8	6.1	5.5	5.7	3.8	5.7	1.7
CPM	14.2	14.2	1.3	–	4.0	–	–	0.4	–
CPM1A	12.1	12.1	7.5	3.7	3.3	2.0	1.6	2.1	1.0
CPM1A1C	17.6	18.5	16.9	7.5	5.2	5.1	3.7	5.0	2.2
CPM1A2C	19.4	21.9	19.7	8.0	5.5	5.7	4.1	5.7	2.3
CPM1A2.5C	10.0	10.0	6.3	2.3	3.0	1.5	1.1	1.9	0.7

F_L – highest value of the load in the interval (CMOD) of 0.05 mm.
F_M – maximum load of composite.
$F_{R,1}$ and $F_{R,4}$ – residual loads corresponding to the deflections δ_{R1} = 0.46 mm and δ_{R4} = 3.00 mm; $f_{fct,L}$ – stress corresponding to F_L.
$f_{eq,2}$ and $f_{eq,3}$ – equivalent flexural tensile strengths.
$f_{R,1}$ and $f_{R,4}$ – residual flexural tensile strengths.

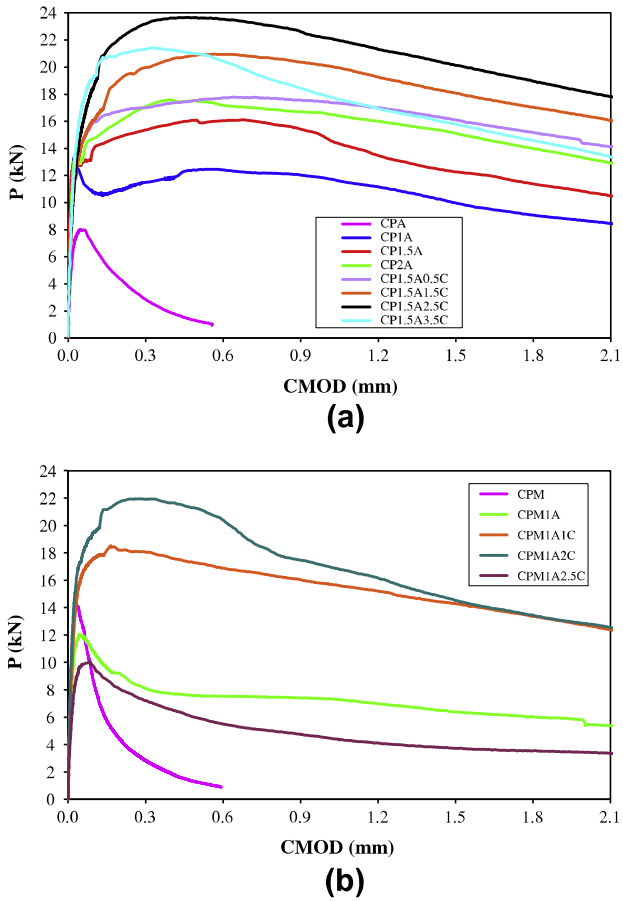

Fig. 5. P-CMOD curves of cement-based composites.

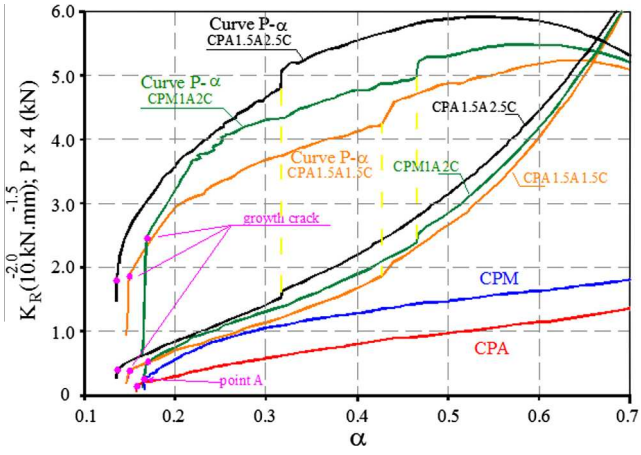

Fig. 6. Composites performance.

Regarding the composite cement-based microconcrete, the resistance value ($f_{fct,L}$) for the composite CPM1A decreased when compared to the composite CPM. This revealed that the isolated presence of fiber type A does not improve the contribution of the microconcrete matrix regarding the tensile strength. However, with the incorporation of steel microfibers together with fibers type A, it was possible to verify an enhancement for the values of $f_{fct,L}$. This tendency was verified for the composites CPM1A1C and CPM1A2C, in which, the strength was respectively, 28% and 37% higher than theCPM.

The values of the equivalent flexural strength $f_{eq,2}$ and $f_{eq,3}$, characterize the composites behavior in relation to the fibers performance. In addition, the performance of the composites CPA1.5A, CPA2A, CPA1.5A0.5C, CPA1.5A1.5C, CPA1.5A2.5C and CPM1A2C is highlighted. In these composites, the action of steel fibers has increased the level of the material strength so that the equivalent flexural strength ($f_{eq,2}$) exceeded the strength value given by the contribution of the matrix ($f_{fct,L}$) only.

2.3.2. P-CMOD curves

In order to represent every composite behavior, the average curve with an intermediary behavior that could be representative for the other two curves of the group was selected among the three curves obtained per group.

In Fig. 5, the P-CMOD average curves for composite cement-based mortar and microconcrete are presented respectively. The uneven behavior between the curves increased even more remarkably after the matrix rupture, i.e., when the contribution of fibers became more effective. The increase in the volume of fibers type A provided a gradual improvement in the ductility of these composites. Considerably, the incorporation of microfibers C together with fibers type A contributed even more.

2.3.3. Fracture resistance curves

In Fig. 6, the curves of resistance obtained for the mortar composites CPA1.5A1.5C and CPA1.5A2.5C are compared with the curve of the microconcrete CPM1A2C. In the mentioned figure, K_R is the fracture resistance and α is the crack depth (a) relatively normalized at the height (W) of the prismatic specimen, i.e., $\alpha = a/W$. Fig. 6 also presents the curves of resistance for the mortar and microconcrete with fibers together with the history loading throughout the process of rupture.

For the prismatic specimens indicated in Fig. 3, the values of K_R were obtained from the pairs (P-CMOD) using Eq. (1), which is valid for beams submitted to the Mode I fracture. In this equation, P represents the applied load, B is the width and S is the clear span of the beam. The geometry-dependent function, $f(\alpha)$, has been determined using two-dimensional plane stress analysis following the procedure of [8,9].

$$K_R = \frac{1.5PS\sqrt{\pi a}}{BW^2} f(\alpha) \quad (1)$$

As shown in Fig. 6, from the point where the growth process of the cracks begins in the matrix for the composites CPA1.5A1.5C, CPA1.5A2.5C and CPM1A2C, one may observe an eminent increase of the resistance to fracture. For example, analyzing the top of the crack at 70% from the section height, one may conclude that the fracture resistance reaches values up to four times higher than verified at 1/3 from the section height.

The exceptional gain in the resistance of these three composites was approximately similar, with a slight superiority for the mortar composite CPA1.5A2.5C, followed by microconcrete CPM1A2C and CPA1.5A1.5C. The development of resistance gain to fracture occurred for each composite following the two well defined stages: the cracking initial stage (before the yellow dashed line), where it was verified a slight increase of toughness to fracture, and the cracking final stage (after the yellow dashed line), where the fracture resistance increased more pronouncedly.

In the initial stage, the tensile process of steel fibers and microfibers and the stress transference among crack surfaces through these fibers begin. In this stage, in which the formation of the cracked surface occurs, it is observed that the crack develops more than the material resistance gain to fracture. A considerable increase in fracture resistance for the composite due to the pulling out of fibers, which are anchored to the cement matrix, was verified in the last stage of the cracking process. At this stage, the efficiency of fibers in relation to the contribution for the increase of fracture toughness is notably reflected.

Table 3
Characteristics of beams.

Beams	Characteristics
V1A	RC beam. Without strengthening. Control
V1C	RC beam model strengthened by three layers of CFRP-sheets
V2C	The tensile zone was demolished and retrofitting with high performance cement-based. RC beam model retrofitting and flexural strengthened by three layers of CFRP-sheets

2.3.4. Flexural tests on three points: brief conclusions

Among the thirteen composites analyzed, it has been possible to conclude that CPM1A2C is the most appropriate material for repair and reconstruction of the transition substrate for bonding the CFRP sheets. This composite has presented a pseudo-hardening behavior, evidenced by the expressive strength gain until an elevated crack width (approximately 0.40 mm) and by the significant gain of tenacity after the matrix cracking. This composite also has shown an elevated gain against fracture even in the initial stage of cracking and essentially during the process of pulling out of the fibers. The behavior of the composite CPA1.5A2.5C should also be highlighted once it has presented a performance slightly superior to composite CPM1A2C. However, it should be observed that the mortar composite has a higher volume of fibers and microfibers when compared to the microconcrete composite.

3. Retrofitting and strengthening of tensile zone of RC beams

3.1. Characteristics of the beams

Three RC beams have been molded with a rectangular section of 170 mm × 350 mm, total length of 3600 mm and free span of 3200 mm. The lower longitudinal reinforcement of beams consisted of two steel bars type CA50 with a 12.5 mm diameter. The upper reinforcement was composed of two steel bars type CA50 with a 6.3 mm diameter. The transversal reinforcement was formed by stirrups with steel bars type CA50 of a 6.3 mm diameter, evenly spaced at every 120 mm. The main characteristics of each beam are described in Table 3.

As reference for the experimental research, beam V1A (without strengthening) has been adopted. From this reference beam it was possible to establish considerations related to the increment of resistance and stiffness provided by the strengthening in the other beams. The reference beam V1A was designed so that there was no crushing of compressive concrete before the steel yields, i.e., ductile behavior.

Beam V1C was flexural strengthened through the application of three sheet layers of CFRP. The strengthening was designed with the goal of detecting the premature debonding of the sheets, a situation assumed if the force in the strengthening cannot be sustained by the substrate. The design of the strengthening was developed using the recommendations available in Ref. [11], in a way that the debonding always occurs before the crushing of the concrete or the failure of the CFRP sheets.

Beam V2C had its tensile zone demolished and subsequently reconstructed by applying a high performance cement-based composite CPM1A2C (Fig. 7). In that way it has been possible to compare the performance of this alternative procedure with the conventional procedure used for strengthening the other RC beams. The cut depth used for the extraction of the concrete in the tensile zone was defined in 80 mm, i.e., 40 mm above from

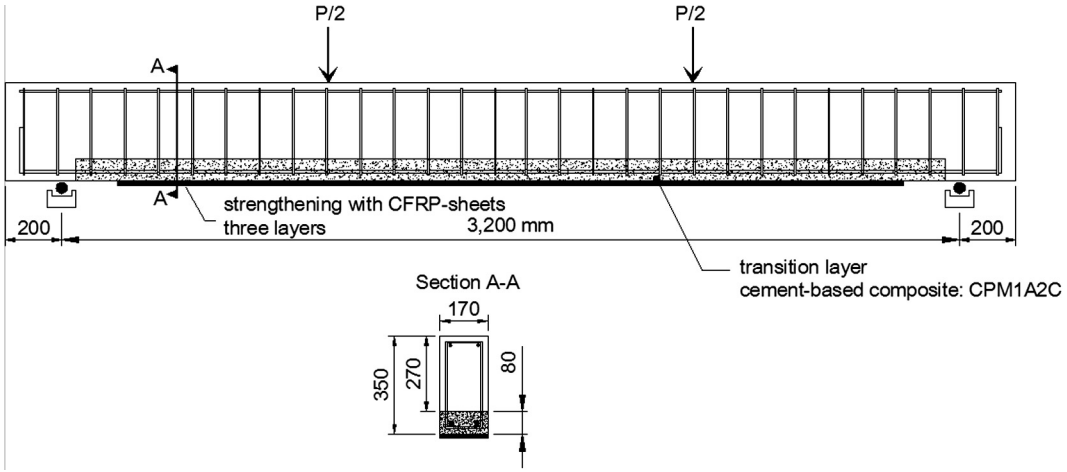

Fig. 7. Schematic of the beam V2C.

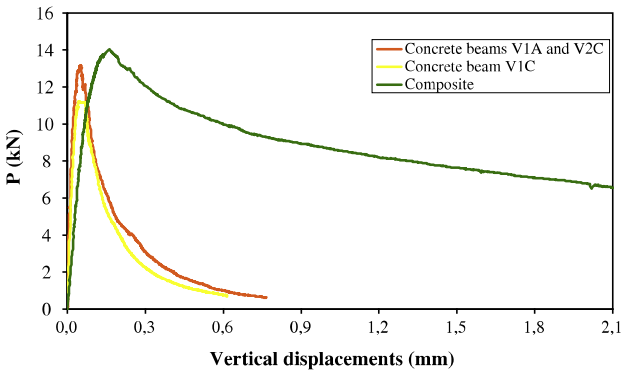

Fig. 8. Curves P–δ for the concrete and composite.

(a)

(b)

Fig. 9. Removal of concrete from the tensile zone of the beam V2C.

the longitudinal reinforcement. This procedure facilitates the treatment of the reinforcement if necessary as well as the anchorage of the new material with the existent stirrups.

3.2. Material properties

Cylindrical specimens of 100 mm in diameter and 200 mm in height were tested in order to obtain the elastic modulus and the compressive strength of the concrete and the composites. The concrete used for molding the beams had characteristic compressive strength of 25 MPa.

Beams V1A and V2C were molded at the same time while beam V1C was molded later. The ages for the beams during the tests were 44 days for the beam V1A, 49 days for the beam V1C and 125 days for the beam V2C. The compressive strength for the beams V1A, V1C and V2C during the tests was 38 MPa, 34 MPa and 39 MPa, respectively. The elastic modulus for the beams V1A, V1C and V2C were 30 GPa, 27 GPa and 29 GPa, respectively. For the cementitious composite, the compressive strength and their elastic modulus were 28 MPa and 29 GPa, respectively, for the age test of the beam V2C.

For the determination of the tensile behavior of the concrete and the cementitious composite, prismatic specimens of 150 mm × 150 mm × 50 mm were molded and tested using the classical three point bending test. The specimens had a central notch and a careful control of the CMOD was applied during the application of the load made by a hydraulic jack Instron of 100 kN capacity. Fig. 8 presents the curves load versus displacement in the middle of the spans (δ) for the flexural behavior of the concrete and the cementitious composite.

Standard reinforced steel bars with a characteristic strength of 548 MPa and an elastic modulus of 211 GPa were used for the longitudinal reinforcement of the beams V1A and V2C. Steel bars with a characteristic strength of 532 MPa and elastic modulus of 200 GPa were used for the longitudinal reinforcement of the beam V1C.

Table 4
Properties of the CFRP.

Epoxi adhesive	Commercial name	*Sikadur 330*
	Color	Part A – white/Part B – gray
	Tensile strength	30 MPa (7 days)
	Tensile strain	0.009
	Bending modulus	3800 MPa
	Tensile modulus	4500 MPa
	Moisture	4:1 – A:B (weight)
	Consumption	1.0 a 1.5 kg/m^2
Carbon fibers sheet	Commercial name	*SikaWrap – 300C*
	Weight	300 g/m^2 ± 15 g/m^2
	Thickness	0.166 mm
	Density	1.79 g/cm^3
	Tensile strength	3900 MPa
	Elastic modulus	230 GPa
	Failure strain	0.015

Tensile test results of mechanical properties of carbon fibers:
Tensile strength: 3100 MPa.
Failure strain: 0.013.
Elastic modulus: 234 GPa.

3.3. Retrofitting of tensile zone and application of strengthening on beams

The procedures to remove concrete and retrofit and strengthen the tensile zone of beam V2C were initiated when the concrete was 23 days old. The concrete removal was mechanically performed with an electric jackhammer (10 kg) and concluded with a sledgehammer, pointer and chisel (Fig. 9). To prepare the tensile zone with composite CPM1A2C, two molds of plasticized plywood were positioned on the two sides of the beam. The composite was manually placed into the molds.

It is important to register that the procedures adopted for reconstructing the substrate of the beam V2C have been facilitated by the fact that the tensile chord of the beam was positioned upwards. The concrete surface of the mentioned beam was kept almost dry while the internal structure was kept wet, i.e., in the saturated condition. This action was adopted in order to avoid the excessive absorption of water by the surface to be repaired. The formation of a film of water on the surface of the beam was also eliminated in order to avoid any problems regarding the anchorage of the cementitious composite.

As mentioned before, the tensile chord of the beam was positioned upwards. This position enhances the shear resistance in the interface between the substrate and the cementitious composite. This enhanced behavior would not be possible if the beam were repaired in the normal position found in the practice, i.e., the tensile chord positioned in the downward position. As the main objective of this research is to evaluate the performance of the cementitious composite for repairing and strengthening, the position of the tensile chord is supposed to be a minor issue in this paper.

The general methodology used for the application of strengthening on the beams V1C and V2C is detailed in Ref. [5] and it should be highlighted that the repair is constituted by three layers of CFRP. The epoxy adhesive used was Sikadur 330 and the sheet was SikaWrap 300C, both, provided by Sika (Table 4). Fig. 10 shows the layer aspect after its reconstitution and the strengthening.

The strengthening was conducted in the beam V1C when the concrete was 41 days old. By another hand, the strengthening was conducted in the beam V2C when the concrete and the cementitious composite was 118 and 91 days old, respectively.

3.4. Testing procedures

The RC beams were tested using a simple, four pointing bending test by means of a monotonic loading up to failure. The structural

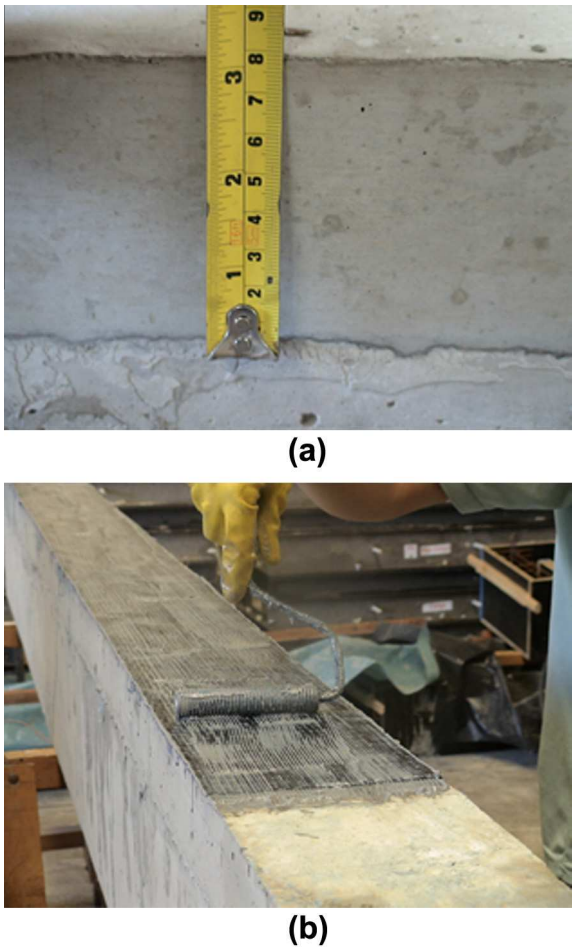

Fig. 10. Tensile layer aspect after the retrofitting and strengthening.

behavior of beams has been observed and monitored throughout the tests, by recording the loads, and the corresponding vertical displacements and the deformations of concrete, steel and strengthening material.

The test setup was mounted in the Laboratory of Structures at the Engineering School of São Carlos, as illustrated in Fig. 11. The load was applied through an actuator servo hydraulic (Instron) with 500 kN of nominal capacity, able to control the intensity and the speed of loading as well as the displacements.

The beams were subjected to displacement-control of the actuator piston with the imposition of a rate of 0.007 mms. The actuator remained attached to a metallic beam of great stiffness, part of a reaction porch at the center of the beam. For monitoring the specific deformations of the reinforcement and the strengthening, strain gauges (*Vishay Micro-Measurements*) with resistance of 120.0 OHMS and 12 mm length have been used. The nomenclature and scheme for positioning the instrumentation of the beams are indicated in Fig. 12.

4. Test results

4.1. Failure modes

As expected, the failure mode of the beam V1A was characterized by an excessive deformation of the longitudinal reinforcement, followed by high deformations in the compressive zone.

The failure of beam V1C (Fig. 13a) has started from the appearance of a crack at the strengthening end (P = 117 kN). The propagation of this crack occurred in the horizontal direction and

Fig. 11. Schematic situation of the tested beams.

culminated in the debonding of the strengthening accompanied by all the concrete cover for the reinforcement situated in the shear span (1066 mm). This type of failure is named plate end debonding (PE), as described by Ref. [12], wherein the debonding cracks initiate at the strengthening ends and propagate inwards.

The failure of beam V2C (Fig. 13b) was different from that one observed for beam V1C. This variance in the failure mode results from the tougher tensile transition layer. Although a crack has appeared at the strengthening end when the applied load was 141 kN, this crack has not propagated horizontally. The results clearly show that the transition layer was efficient once it has changed the failure mode of beam V2C and the limit of loading where the debonding was registered.

Failure of beam V2C has been originated from a section located in the shear span and near to the application of the concentrated load. The appearance of a flexural/shear crack and the development of its opening with the increment of load, cause the strengthening debonding through the cement composite interface with the epoxy adhesive until its nearest end. A thin layer of microconcrete remained jointed to the sheet.

For the beam V2C, an intermediate crack caused the strengthening to debond. As described by Ref. [10], this behavior is referred as an intermediate crack (IC) debonding and it is associated with the strains in the strengthening.

4.2. Loads

The values of the cracking load (P_f), yielding of the longitudinal reinforcement (P_y) and failure loads (P_u) of the tested beams are shown in Table 5. The presence of strengthening increased the first crack load of the strengthened beams. The increment was of 19.8% for the beam V1C and 66.2% for the beam V2C. In relation to the beam V1C, the cracking load of the beam V2C was increased by 38.8%.

The presence of strengthening also increased the load necessary for the yielding of the longitudinal reinforcement. This occurred because the strengthening assists the steel reinforcement to resist to tensile stresses. For the beam V1C, the increase was of 48.4% while in the beam V2C the increase reached 67.1%.

Regarding the ultimate load it is highlighted by the response of the beam V2C. A significant increment of 120% was observed in relation to the control beam, while the beam V1C presented a limited increment of 65.1%. Considering the strengthened RC beam, the resistance capacity for the beam V2C was 33.2% higher.

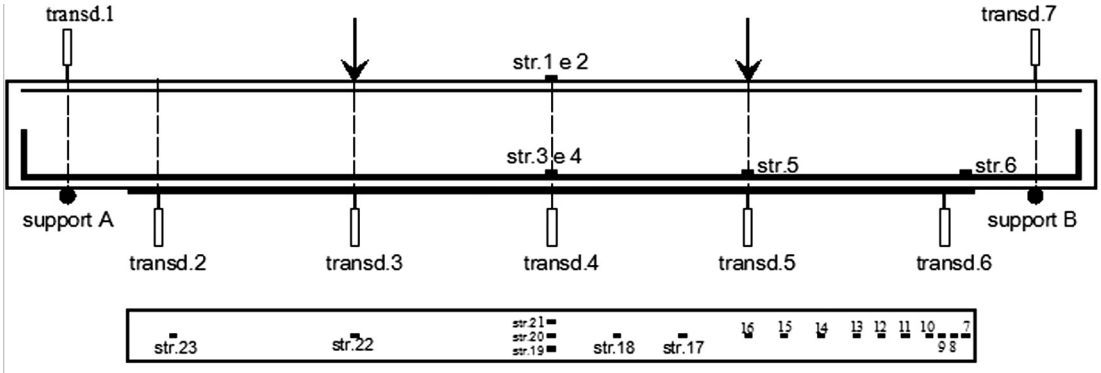

Strain gauges locations:

Strain gauges in the concrete and reinforcement

reference support A	number of strain gauge					
	1	2	3	4	5	6
0.0 mm	1600	1600	1600	1600	2250	2970

transd. = transductor
str. = strain gauge

Strain gauges in the strengthening

reference support A	number of strain gauge																
	7	8	9	10	11	12	13	14	15	16	17	18	19	20	21	22	23
0.0 mm	2970	2930	2890	2850	2770	2690	2610	2490	2370	2250	2034	1818	1600	1600	1600	950	350

Fig. 12. Nomenclature and positioning of the strain gauges and LVDT'S.

(a)

(b)

Fig. 13. Failure modes of beams V1C and V2C.

4.3. Vertical displacements

Fig. 14 presents the load–deflection curves (P–δ) for the beams V1A, V1C and V2C. It is possible to observe that the behavior of the beams is very similar until the cracking load. After the cracking, it is clear that there is an increase in the stiffness of the strengthened beams when compared with the beam without strengthening. The contribution of the transition layer in the responses of the beam V2C is emphasized, once higher stiffness and load capacity were obtained especially in relation to the beam V1C.

For the beam V1A, any addition of loading after the yielding of the longitudinal reinforcement was obtained. On the other hand, for the strengthened beams, there was clearly observed an increase of loading after the yielding of the longitudinal reinforcement. In this way, the largest extension for the final stretch of the curve of beam V2C indicates that the strengthening was more required in this beam than in the beam V1C.

Table 5 presents a comparison between the deflections in the middle of the span for a load equal to 90% of the failure load of the beam V1A. The values show that the strengthened beams were

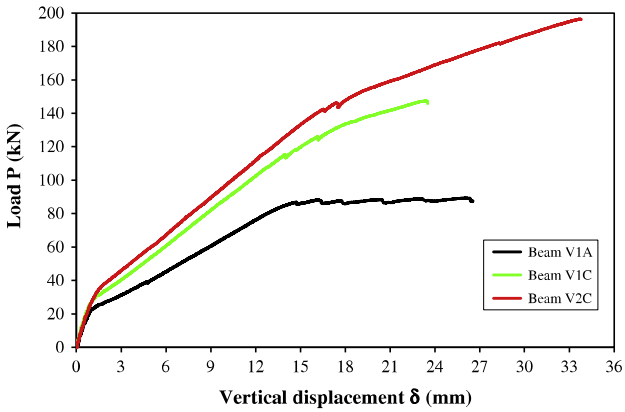

Fig. 14. Load–deflection curves of the beams V1A, V1C and V2C.

stiffer than the control beam. The deflection of the beam V1C corresponds to 68% of the beam V1A.

The beam V2C presented a deflection even less pronounced than the beam without strengthening. The deflection of this beam was equal to 60% than the beam V1A. Therefore, the procedure proposed in the present paper (retrofitting and strengthening of the tensile zone) is not only effective in terms of load capacity, but also in terms of stiffness.

4.4. Stresses and strains

The strengthening response of a beam is evaluated in here through the distribution of specific strain throughout its extension. By associating the strengthening geometric and mechanical properties to values of strain, it is possible to obtain a distribution of longitudinal and bond stresses along the strengthening. Eq. (2) gives the bond stresses for the strengthening along the instrumented points:

$$\tau_r = \frac{\varepsilon_{r(i+1)} - \varepsilon_{r(i)}}{s_{(i+1)} - s_{(i)}} \cdot E_r \cdot t_r \tag{2}$$

where τ_r is bond stress (MPa); ε_r is strain in the strengthening; s_i is relative position of the strain gauge (mm); E_r is modulus of the strengthening (MPa); and t_r is thickness of the strengthening (mm).

In Figs. 15 and 16 are presented the profiles of normal and bond stresses along the strengthening of the beams V1C and V2C, respectively, for rates of 25%, 50%, 75% and 100% of the ultimate load. From the general analysis of these figures it is possible to verify that the maximum values of normal stresses were recorded in the central region of the beams. For beams V1C and V2C the maximum value of normal stresses occurred at 218 mm of the middle of the span and was recorded through strain gauge 18.

For the beam V1C, the maximum normal stress (1239 MPa) recorded in the strain gauge number 18 is equivalent to a deformation in the strengthening equal to 0.0053. From the profile of stresses, it was possible to find significant values of the normal stresses (in the order of 450 MPa) as well the concentration of the higher values for the bond stresses in the strengthening end

Table 5
Loads, failure modes and comparative of beams deflections.

Beams	Loads (kN)			Failure mode	Increments (%)			Deflection (mm)
	P_f	P_y	P_u		P_f	P_y	P_u	
V1A	21.0	79.8	89.3	Excessive deformation for the longitudinal reinforcement	–	–	–	12.79
V1C	25.2	118.5	147.4	Strengthening debonding	19.8	48.4	65.1	8.73
V2C	34.9	133.4	196.4	Strengthening debonding through the cement composite interface	66.2	67.1	120.0	7.68

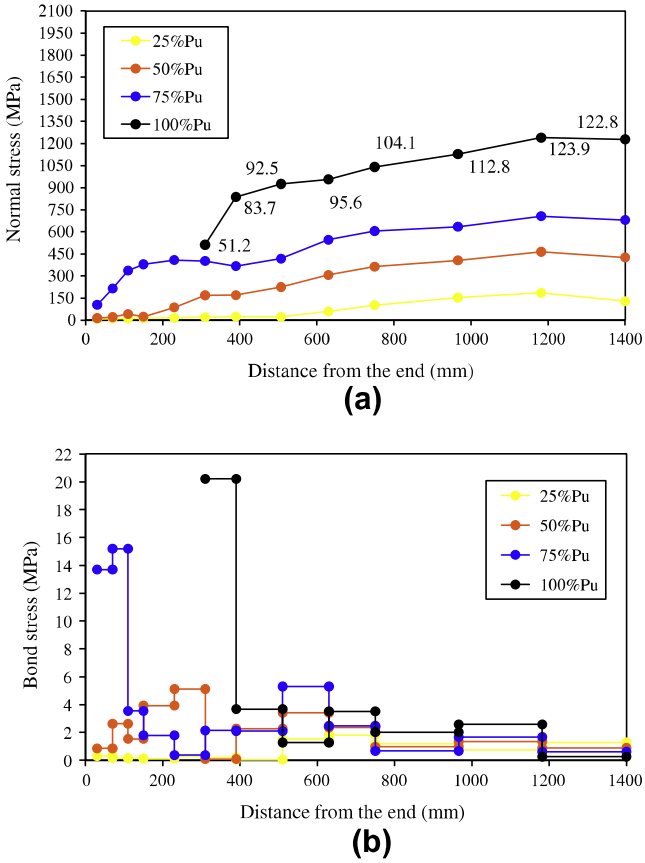

Fig. 15. Distribution of normal and bond stresses in the beam V1C.

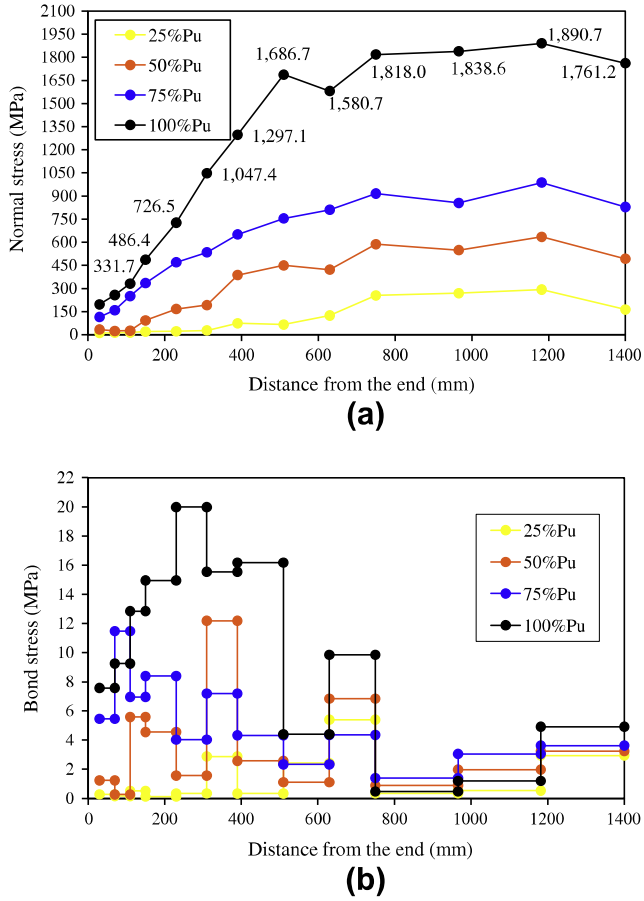

Fig. 16. Distribution of normal and bond stresses in the beam V2C.

for 75% and 100% of the ultimate loading. The high values of bond stress developed at the end of the strengthening of the beam V1C shows that the failure occurred by plate end debonding (PE). This type of failure is characterized by debonding cracks that initiate in the end of the strengthening and propagate inward.

For the beam V2C the distribution of normal and bond stresses along the strengthening (Fig. 15) indicates maximum values of 1891 MPa and 20 MPa, respectively. The maximum normal stress, which is equivalent to a strain in the strengthening of 0.0081, was recorded by the strain gauge number 18 and the maximum bond stress was given by the strain gauge number 11.

The failure mode observed for the beam V2C is characterized by the high values of normal stress registered in the strain gauges 14, 15 and 16. The mentioned strain gauges were located in the shear span, between 600 and 800 mm of the strengthening end, where an intermediate crack caused the debonding. As one may observe in Fig 15, the deformation registered in the strengthening was significant due to this intermediate crack, taking into account the flexure and shear actions. The high value of bond stress developed at the end of the shear span reveals the propagation of a horizontal crack interface. This crack is initiated from the interception of the intermediate crack/strengthening and propagates to the end of the strengthening.

5. Analysis using Finite Element Method (FEM)

5.1. Discretization

The nonlinear behavior of the beams V1A, V1C and V2C were also simulated using the package software Diana, version 9.1,

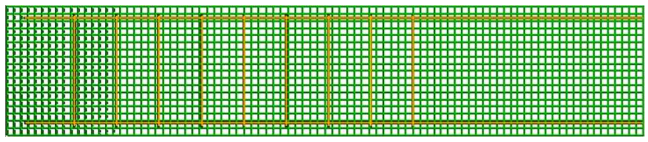

Fig. 17. Finite element model of strengthened RC beams.

based on the Finite Element Method (FEM). Fig. 17 presents the finite element mesh used for the beams, including the arrangement of the reinforcement. This mesh was constructed using quadratic elements of 8 nodes type CQ16 M while the longitudinal and transversal reinforcement were modeled using embedded reinforcement elements with perfect bonding, i.e., eliminating the possibility of rupture by slippage of the bars. The nodes of finite elements, representative of the external strengthening, were connected with the adjacent nodes of the concrete elements simulating a perfect bond between the materials.

The constitutive models and the mechanical properties of material used in the nonlinear analysis of the beams V1A, V1C and V2C are detailed in Table 6.

The values of tensile strength (f_c in MPa) considered for concrete, were those obtained according to ACI [13] through the equation: $0.332 \cdot (f_c)^{1/2}$. The values of crack bandwidth were taken considering the square root of the finite element area, according to the recommendation in the Diana [14].

The presence of the transition layer in the beam V2C was established through a plane surface located in the tensile zone of the model. The bond between the transition layer and the surface representative of the adjacent concrete was considered perfect. The

Table 6
Materials and parameters for the numerical model of the beams V1A, V1C and V2C.

Concrete
Linear elasticity: Isotropic, Young's modulus: (V1A = 30 GPa, V1C = 27 GPa and V2C = 29 GPa), Poisson's ratio = 0.20 *Static nonlinearity:* Concrete and brittle materials, total strain rotating crack, direct input, exponential softening in tension, ideal in compression Tensile strength: (V1A = 2.0 MPa, V1C = 1.9 MPa and V2C = 2.1 MPa) Mode-I tensile fracture energy: (V1A = 0.15 N mm/mm^2, V1C = 0.12 N mm/mm^2 and V2C = 0.16 N mm/mm^2) Crack bandwidth = (finite element area)^{0,5}: (V1A = 19.61 mm, V1C = 20.12 mm and V2C = 20.03 mm) Compressive strength: (V1A = 38 MPa, V1C = 34 MPa and V2C = 39 MPa)
Steel bars (longitudinal reinforcement) *Linear elasticity:* Reinforcement, reinforcement bonded, Young's modulus: (V1A/V2C = 211 GPa and V1C = 200 GPa) *Static nonlinearity:* Reinforcement, VonMises plasticity, ideal plasticity, yield stress: (V1A/V2C = 548 MPa and V1C = 532 MPa)
CFRP *Linear elasticity:* Isotropic, Young's modulus = 234 GPa
Finite element mesh Eight nodes rectangular elements CQ16 M: (V1A = 1638; V1C = 1809 and V2C = 1981). Nodes: (V1A = 5133 nodes; V1C = 5648 and V2C = 6188) Plane stress

Table 7
Materials and parameters referring to the transition layer of the beam V2C.

Numerical model V2C – composite cement-based CPM1A2C
Linear elasticity: Isotropic, Young's modulus = 29 GPa, Poisson's ratio = 0.20 *Static nonlinearity:* Concrete and brittle materials, total strain rotating crack, direct input, exponential softening in tension, ideal in compression, tensile strength = 2.2 MPa, Mode-I tensile fracture energy = 0.53 N mm/mm^2, crack bandwidth = (finite element area)$^{0.5}$ = 20.03 mm, compressive strength = 28 MPa

mechanical properties of the transition layer of beam V2C were taken from the characterization values of the cement composite and are indicated in Table 7.

The values of tensile strength assumed for the cement composite were obtained through RILEM TC 162-TDF [10] using the equation: $0.6 \cdot f_{fct,L}$. The post-peak behavior of the cement composite was represented by an exponential softening in tension diagram,

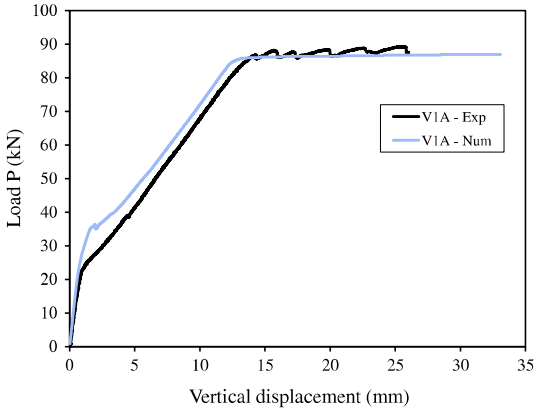

Fig. 18. Beam V1A: experimental and numerical curves.

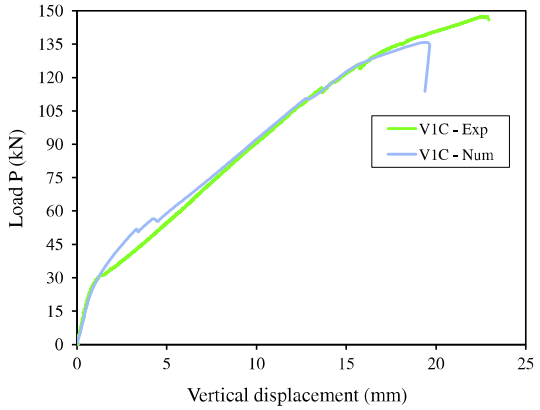

Fig. 19. Beam V1C: experimental and numerical curves.

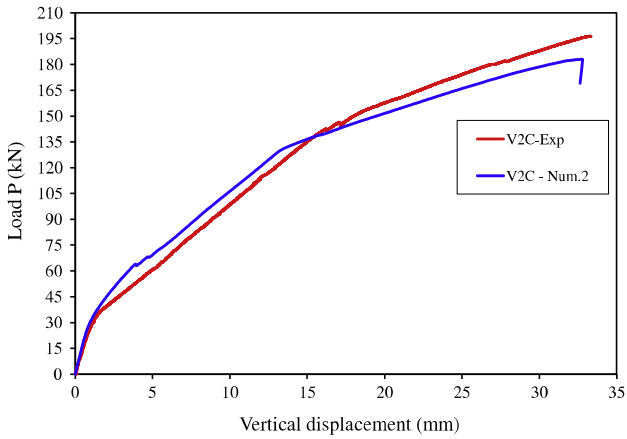

Fig. 20. Beam V2C: experimental and numerical curves.

and the high value attributed to the fracture energy is due to the presence of fibers and microfibers of steel. The fracture energy was calculated up to a deflection of $\delta = 2.65$ mm of the prismatic specimen.

5.2. Numerical analysis results

In Fig. 18, curves load–deflection obtained by means of numerical simulations are compared with those obtained from experimental research of the beam V1A. From this figure it is possible to verify that, in the elastic phase, the numerical curve for the control beam is identical to the experimental curve and after concrete cracking, the numerical curve is stiffer. For the yielding of the reinforcement, both curves approach again.

For the control beam, the first crack load obtained numerically is 24.6 kN, which is 17% higher than the load 21.0 kN obtained experimentally. The yielding of the reinforcement longitudinal occurred for a load of 85.3 kN and a sharp drop of the stiffness was observed. The numerical yielding load was 6.89% higher than the experimental yielding load (79.8 kN).

From Fig. 19, it is possible to visualize that the behavior of both curves (numerical and experimental) are very similar for the beam V1C. After the concrete cracking and up to the load of 75 kN, the numerical curve is slightly more stiff than the experimental curve. After this loading value, the curves develop again very similarly up to approximately 128.6 kN. Above this loading value up to the failure, the numerical curve develops with a stiffness regarding the experimental curve.

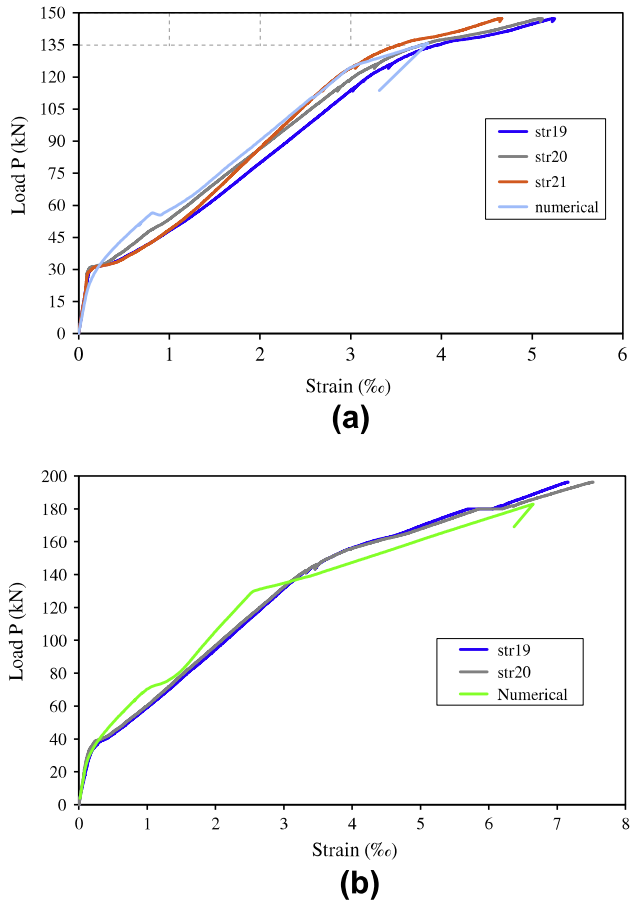

Fig. 21. Numerical and experimental strains in the middle of the strengthening (a) V1C and (b) V2C.

The first concrete crack obtained through the FE occurred with load equal to 27.0 kN, this value being 7.15% higher than the one obtained experimentally. The yielding of reinforcement, according to the numerical model was given by a load of 122.4 kN, i.e., only 3.33% above the experimental value which is 118.5 kN. In addition, the load value corresponding to the failure pointed by the numerical model is 134.3 kN, while the experimental is 147.4 kN.

Fig. 20 shows that until the yielding of the reinforcement, the numerical curve shows a higher stiffness in regard to the experimental curve. After the yielding of the reinforcement, the numerical curve begins to show higher values of vertical displacements within a similar level of loading.

The first crack appearance according to the experimental results was given by a load of 34.9 kN, while by the numerical model was given by a load of 32.2 kN. The yielding of the reinforcement according to the experimental results occurred at a load of 133.4 kN, while the numerical model indicated a yielding at a load of 129.6 kN. This value is 2.88% lower than the one obtained experimentally. As for the failure of the beam V2C, the numerical model had a value of load of 182.9 kN, while the experimental value was 196.4 kN.

In general, the numerical curves of load–deflection for the control beam and strengthened beams presented a good concordance with the experimental curves. In the elastic phase, the behavior of the beams was practically identical, except for the curve of model V2C, a little more rigid than the experimental curve.

Until the yielding of the reinforcement, the numerical curves were stiffer than the experimental curves. Additionally, after the yielding of the reinforcement, the deflections represented by the models of the strengthened beams were more pronounced than the experimental results.

Fig. 21 illustrates the development of strains in the strengthening obtained experimentally and by means of numerical analysis. The values of strain refer to the middle section of the beam. For the beam V1C, the values of numerical strains of the strengthening in the middle of the span were highly correlated with the experimental values. Even after the concrete cracking and the yielding reinforcement, the development of numerical strains represented the experimental results satisfactorily. Until the yielding of the reinforcement, the numerical curve was slightly more inclined than the experimental curves. After the yielding of the reinforcement, the numerical strains of strengthening developed more pronouncedly and thereafter the failure occurs.

In Fig. 21b, one may observe that the numerical model reflects the development of experimental strains in the strengthening of the beam V2C. Before the yielding of the reinforcement, the numerical curve is more inclined than the experimental curve. Even after the yielding of the reinforcement, the numerical curve develops similarly to the experimental strains.

The numerical cracking pattern obtained for the beam V1C is characterized by the deterioration of the concrete cover in the

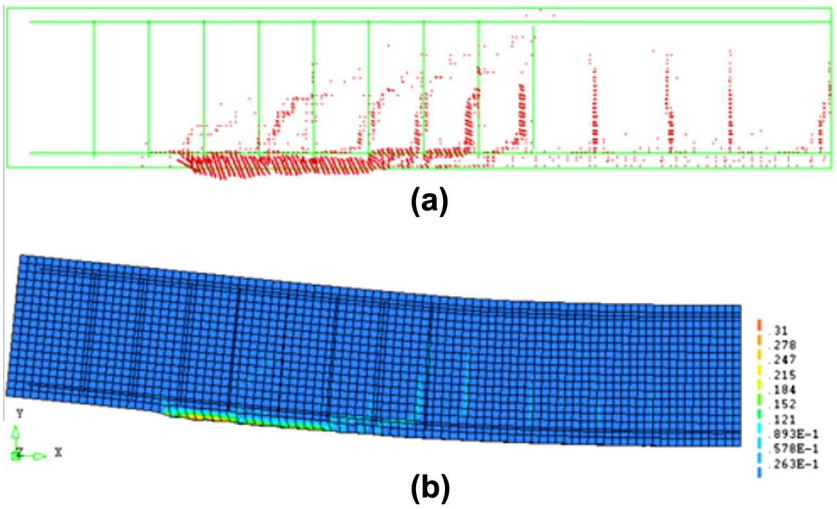

Fig. 22. V1C: failure pattern for the numerical model (a) cracking pattern at failure for the numerical model and (b) deformed shape and tensile principal strains at failure.

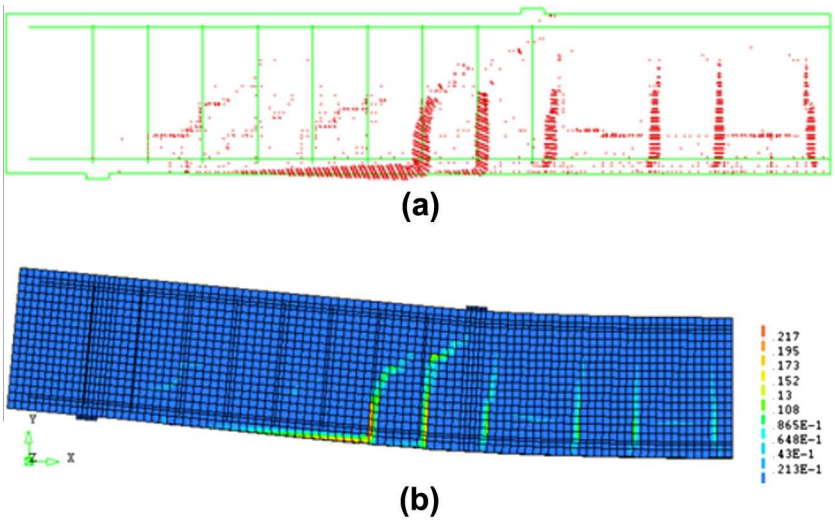

Fig. 23. V2C: failure pattern for the numerical model (a) cracking pattern at failure for the numerical model and (b) deformed shape and tensile principal strains at failure.

shear span. As indicated in Fig. 22a very intense cracking may be observed between the strengthening and the longitudinal reinforcement. The failure mode described by the numerical model clearly represented the experimental failure mode.

The numerical cracking pattern obtained for the beam V2C clearly reveals a shear/flexure crack for a section positioned in the shear span, in the vicinity of the point of application of the concentrated load, as shown in Fig. 23.

The failure modes PE and IC are numerically represented by Figs. 22 and 23, respectively. These numerical results are helpful to better understand the results obtained experimentally. The effect of the substrate transition for the beam V2C is well evidenced when Figs. 22a and 23a are compared.

The fracture strength developed by the steel fibers and microfibers has avoided the cracking failure of the transition substrate that constitutes the lower chord of beam V2C. In this beam, the failure process of the transition substrate is related to the pulling out of fibers from the cementitious matrix. This phenomenon has not occurred and failure was due cracking in the interface constituted by the substrate and the strengthening.

6. Conclusions

This research aimed at proposing a constructive technique for the flexural strengthening of RC beams. This technique involved a process of previous retrofitting of hypothetically damaged beams with a high performance composite based on Portland cement and short steel fibers specially developed to enhance the strength of the transition layer.

The experimental and numerical results have shown that the proposed technique (even with the possibility of further improvements, as any other technique) may be efficient both in the reconstitution of tensile zone of RC beams as well as for the improvement of the performance as a whole, especially when using CFRP sheets as a strengthening solution.

Based on the experimental and numerical results obtained previously, these main conclusions may be drawn:

- the addition of steel microfibers together with conventional fibers enhances the contribution of the matrix to the composite strength and the mechanism of stress transfer from matrix to fibers;
- with the matrix cracking, the stress transfer was facilitated by the steel microfibers, which in the matrix, led to the progress of cracking with the increase in the loading level;
- the flexural strengthening of beams through the external bonding of CFRP sheets to a transition layer constitutes an efficient strategy with practical application in engineering;
- the previous reconstitution of tensile zone with a high performance cement-based composite based on macro and microfibers of steel prevents the rapid progression of a critical crack at the strengthening end and delays the sheet debonding;
- the presence of a material with greater fracture strength in the tensile zone of the beam, promotes cracks that become more distributed and with small openings along the strengthening extent;
- besides the considerable increase in resistance, the bonding of CFRP sheets to a transition layer leads to a significant increase of beam stiffness in relation to a beam without a transition layer;

Finally, it is worth highlighting that the proposed methodology is still under development and new improvements must be made to the initial procedures. Despite the initial good results, new research should be conducted, intending to better develop the methodology for obtaining cement-based composites with higher flexural strength and fracture energy. Also, the behavior of the transition zone constructed using the mentioned composites and CFRP needs to be better explored.

Acknowledgments

We thank FAPESP and CAPES for financial support. We also thank Maccaferri–Latin America for the production, under purchase order, of steel microfibers.

References

[1] Chen JF, Teng JG. Shear capacity of FRP-strengthened RC beams: FRP debonding. Constr Build Mater 2003;17(1):27–41.
[2] Maalej M, Bian Y. Interfacial shear stress concentration in FRP-strengthened beams. Compos Struct 2001;54:417–26.
[3] Leung CKY. FRP debonding from a concrete substrate: some recent findings against conventional belief. Cem Concr Compos 2006;28:742–8.
[4] FIB. Bond of reinforcement in concrete-state-of-the-art report. Lauseanne. Bulletin 2000;10.
[5] Ferrari, VJ. Flexural strengthening of reinforced concrete beams with carbon fibers reinforced polymer sheet bonded to a transition layer of high

performance cement-based composite. Ph.D thesis. University of Sao Paulo, School of Engineering; 2007.
[6] Ferreira LET. About the fracture resistance concrete and the steel fibers concrete. Ph.D thesis. University of Sao Paulo; 2002.
[7] RILEM TC 162-TDF. Test and design methods for steel fiber reinforced concrete. Bending test. Mater Struct 2002;35:579–82.
[8] Ferreira LET, Bittencourt TN, Sousa JLAO. Gettu R-curve behavior in notched beam tests of rocks. Eng Fract Mech 2012;32:27–40.
[9] Ferreira LET, Bittencourt TN, Gettu R. Determinação computacional das equações da mecânica do faturamento elástico linear para o corpo de prova de $150 \times 150 \times 500$ mm e análise das implicações decorrentes da determinação experimental do CMOD sobre os parâmetros de faturamento, IV Simpósio EPUSP sobre Estruturas de Concreto, São Paulo, Brazil; 2000. CD-ROM.
[10] RILEM TC 162-TDF. Test and design methods for steel fiber reinforced concrete. Design of steel fiber reinforced concrete using the σ-w method: principles and applications. Mater Struct 2002;35:262–78.
[11] ACI Committee 440. Guide for the design and construction of externally bonded FRP systems for strengthening concrete structures (ACI 440. 2R-08). Michigan: American Concrete Institute; 2008.
[12] Oehlers DJ, Seracino R. Design of FRP and steel plated RC structures: retrofitting beams and slabs for strength, stiffness and ductility. Elsevier; 2004.
[13] ACI 318M-08. Building code requirements for structural concrete. Detroit; 2008.
[14] DIANA – Finite Element Analysis – User's Manual release 9. TNO DIANA BV.P.O. Box 49, 2600 AA Delft, The Netherlands.